Indian J. Phys. **66A** (4), 559-582 (1992)

Transmittance through random media*

Abhijit Mookerjee
S N Bose National Centre for Basic Sciences, DB 17, Sector 1, Salt Lake City, Calcutta-700 064, India

Abstract : We present a tractable and stable technique for numerical determination of transmittance and conductance through random media. The methodology is numerically stable for large systems and capable of being generalised for higher dimensions. We illustrate the technique by two specific applications

Keywords : Transmittance, Azbel resonances, random chains, quasi periodic chains

PACS Nos. : 71.50.+t, 71.55.Ju, 72.15.Eb

1. Introduction

The problem of transmittance through random media is a long standing one. Interest in the problem is spread over a wide range : from the physicists' interest in the conductance of electrons through disordered solids, or the transmittance and reflectance of elastic waves through the earth's crust, of interest to oil or water prospectors, to the passage of starlight through the disordered dielectric media of the universe. In general, analytic solution of the problem is exceedingly difficult, except in the most trivial of models. Nor are analytic attempts free from controversy. The configuration averaged viewpoint, which has been successful in many problems, unfortunately tends to mask the characteristics of individual systems which in many cases dominate the specific system's properties. This is certainly true of resonance properties. It is for this reason that there has been considerable emphasis on the numerical study of disordered systems. However, stable numerical procedures exist by and large for one dimensional systems alone. Either these methods have not been extended to higher dimensions, or those that are available involve numerically unstable procedures involving divergent recursions and matrix inversions.

The aim of this article is to present a numerical procedure which is tractable and stable *and formulated for general dimensionality*. We should like to suggest that the vector recursion method should be tried out in transmittance problems. The technique is relatively fast and numerically stable. We shall also present some applications of the method to bring out the fact that the technique, in contrast to earlier methods, gives unambiguous information.

* The work described in this article is based on the collaborative work of the author with Chaitali Basu, Indra Dasgupta and Tanushree Saha of the S N Bose National Centre and Drs Asok K Sen and Prabhat K Thakur of the Saha Institute of Nuclear Physics, Calcutta, India.

© 1992 IACS

2. The vector recursion method

We shall describe a system through which we wish to study the transmittance by an Anderson tight-binding Hamiltonian of the type described in (1). The chain will be of length $2N$:

$$H_{\text{sample}} = \sum_{n=1}^{2N} \left\{ \varepsilon_n \phi_n^{\dagger} \phi_n + \sum_m V_{nm} (\phi_n^{\dagger} \phi_m + \phi_m^{\dagger} \phi_n) \right\}. \tag{1}$$

To the two ends $n = 1$ and $n = 2N$ we attach elementary, perfectly conducting, semi-infinite *leads*. The purpose of these leads is to bear the incoming, reflected and transmitted waves. Godin and Haydock [1] have shown that in any solid, for instance, since only a finite number of bands cross the Fermi energy, the Hamiltonian of the leads can always be converted to independent elemental chains of the type described below by the use of the simple Recursion method [2]

$$H_{\text{in}} = \sum_{n=0}^{-\infty} \{ \varepsilon' \phi_n^{\dagger} \phi_n + V' (\phi^{\dagger}_{n+1} \phi_n + \phi^{\dagger}_n \phi_{n+1}) \}.$$

$$H_{\text{out}} = \sum_{n=2N+1}^{\infty} \{ \varepsilon'' \phi^{\dagger}_n \phi_n + V'' (\phi^{\dagger}_{n+1} \phi_n + \phi^{\dagger}_n \phi_{n+1}) \}. \tag{2}$$

For simplicity we shall take $\varepsilon' = \varepsilon'' = 0$ and $V' = V'' = V_{\text{lead}}$.

The solution of the Schrödinger equation in the two leads are known. These are travelling Bloch waves of the form

$$\psi_{\text{leads}} = \sum \psi_n \phi^{\dagger}_n \tag{3}$$

with $\psi_n = A\, e^{\mp in\theta}$. As the wave travels through the leads, it phase changes by θ from one site to the next. In the elementary, perfectly conducting leads, this phase change is determinate :

$$\cos\theta = (E / 2V_{\text{lead}}) \tag{4}$$

where E is the energy associated with the incoming wave.

We have assumed that transport is ideal in the leads right upto the contacts with the sample. This ignores boundary effects. However, if we consider large enough samples, such boundary effects are expected to be negligible.

The density of states is non-zero in the region $E_1 \le E \le E_2$. If we wish to examine the transmittance within this band, we must choose a V_{lead}, which allows this full band pass, i.e. $V_{\text{lead}} \ge (E_2 - E_1)/4$. This is because, in order to have propagating states in the leads, we must have a real solution to eq. (4).

The *Vector recursion technique* now changes to a new *vector basis* with vector annihilation operators

$$\Phi_n = \begin{pmatrix} \phi_n^{(1)} \\ \phi_n^{(2)} \end{pmatrix} \qquad \text{with } \Phi_1 = \begin{pmatrix} \phi_1 \\ \phi_{2N} \end{pmatrix}$$

and the others are generated from the recursive formula :

$$B^{\dagger}_{n+1}\,\psi_{n+1} = \{H\,\psi_n\} - A_n\,\psi_n - B_n\,\psi_{n-1} \tag{5a}$$

where $\psi_n = \psi_n\,\Phi_n^{\dagger}.A_n = \psi_n^{\dagger}\,H\,\psi_n$ and B_n is found by disentangling $B^{\dagger}_{n+1}\,\psi_{n+1}$ using the Gram-Schmidt orthogonalisation of its two components.

In this basis, the lead and sample Hamiltonians become :

$$H_{\text{sample}} = \sum_{n=1}^{N}\{A_n\,\Phi_n^{\dagger}\,\Phi_n + B_{n+1}\,\Phi^{\dagger}_{n+1}\,\Phi_n + B^{\dagger}_{n+1}\,\Phi^{\dagger}_n\,\Phi_{n+1}\} \tag{5b}$$

$$H_{\text{leads}} = \sum_{-\infty}^{0} V\,\{\Phi^{\dagger}_{n+1}\,\Phi_n + \Phi^{\dagger}_n\,\Phi_{n+1}\}. \tag{5c}$$

The Schrödinger equation may be expressed as a three term linear difference equation involving the 2×2 matrices A and B, and the wave function *vector* amplitudes

$$\psi_n = \begin{pmatrix} \psi_n \\ \psi_{2N+1-n} \end{pmatrix}$$

$$B^{\dagger}_{n+1}\,\psi_{n+1} = (E\,I - A_n)\,\psi_n - B_n\,\psi_{n-1}. \tag{6}$$

Let us now think of a situation where an incoming wave $\sum e^{in\theta}\,\phi^{\dagger}_n$ is travelling to the right along the input lead. As it reaches the sample it is scattered. A *reflected* wave $\sum r\,(E)\,e^{-in\theta}\,\phi_n^{\dagger}$ travels back in the input lead to the left and a *transmitted wave* $\sum t\,(E)\,e^{in\theta}\,\phi_n^{\dagger}$ travels in the output lead. $r\,(E)$ and $t\,(E)$ are the complex *reflection* and *transmission coefficients*. Since the solution in the leads are known, the boundary conditions in the new *vector* basis are :

$$\psi_0 = \begin{pmatrix} 1+r \\ t \end{pmatrix} \qquad \psi_1 = \begin{pmatrix} e^{i\theta} + re^{-i\theta} \\ te^{-i\theta} \end{pmatrix}. \tag{7}$$

Note here that we have chosen to measure our phases from the basis labelled 0 just outside the joint between the leads and the sample. It is also clear that the way we have numbered the new basis, the reflected and transmitted waves both travel to the left, hence the negative sign in the exponent of the transmitted wave.

The general solution of (6) satisfying these boundary conditions may be written in terms of the two independent family of solutions of (7) $\{X_n\}$ and $\{Y_n\}$, which satisfy

$$\begin{aligned} B^{\dagger}_{n+1}\,X_{n+1} &= (E\,I - A_n)\,X_n - B_n\,X_{n-1} & X_0 &= I, X_1 = O \\ B^{\dagger}_{n+1}\,Y_{n+1} &= (E\,I - A_n)\,Y_n - B_n\,Y_{n-1} & Y_0 &= O, Y_1 = I. \end{aligned} \tag{8}$$

This solution is

$$\xi_n = X_n\,\psi_0 + Y_n\,\psi_1 \tag{9}$$

Direct substitution in (6) and (7) shows that this is indeed the required solution with the correct boundary conditions.

In exactly similar manner we can discuss the case in which the incoming wave

travels to the right in the lead labelled 2. After scattering by the sample the reflected wave travels to the right in lead 2 and the transmitted wave to the left in lead 1. Here $r'(E)$ and $t'(E)$ are the *reflection* and *transmission* coefficients of this new problem, with boundary conditions

$$\psi'_0 = \begin{pmatrix} t' \\ 1 + r' \end{pmatrix} \qquad \psi'_1 = \begin{pmatrix} t' e^{-i\theta} \\ e^{i\theta} + r' e^{-i\theta} \end{pmatrix} \tag{7'}$$

and $$\xi'_n = X_n \psi'_0 + Y_n \psi'_1 \tag{9'}$$

We have a further boundary condition. Since the length of the chain is finite, in the new basis the *vector* chain terminates after N steps, so that

$$\xi_{N+1} = 0 \text{ and } \xi'_{N+1} = 0. \tag{10}$$

If we substitute this in (7), (7'), (9) and (9') we immediately obtain an expression for the scattering *S-matrix*

$$S = \begin{pmatrix} r & t \\ t' & r' \end{pmatrix} = -(X_{N+1} + Y_{N+1} e^{-i\theta})^{-1} (X_{N+1} + Y_{N+1} e^{i\theta}). \tag{11}$$

In the absence of magnetic fields the time-reversal symmetry gives $t = t'$. The S-matrix is symmetric. Finally, the *transmittance* $T(E) = |t(E)|^2$ while the *reflectance* $R(E) = |r(E)|^2$.

3. Applications of the vector recursion technique

3.1. The generalised Aubry model :

Recently there has been considerable effort in understanding the nature of electronic states in quasi-periodic systems. Practical applications of such studies involve, among other things, incommensurate superlattices [3] and one dimensional quasi-crystals [4]. While it is well known that in an one dimensional system with random potentials *all* states are localised [5], and whereas *all* states are extended Bloch states in the absence of disorder, it has recently been shown [6-11] that certain quasi-periodic systems in one dimension are capable showing transition from localised to extended states. In addition, there is interesting behaviour in the intermediate critical states.

A simple quasi-crystalline model is the so called Aubry model where $\varepsilon_n = \lambda \cos(2\pi Q n + \delta)$ [12-14]. Typically the hopping energy V_n is a non-random quantity (= V), set equal to 1 to fix the energy scale. In this case the period Q^{-1} of the potential is incommensurate with the period of the lattice (= 1). When Q is irrational, the spectrum is absolutely continuous (i.e. all states are extended) for $o < \lambda < 2$. It is point-like (i.e. all states are localised) if $\lambda > 2$. In fact, an interesting duality property (Aubry duality) exists between the cases $\lambda < 2$ and $\lambda > 2$, with the case $\lambda = 2$ being self dual. For this last case ($\lambda = 2$), all states are critical and the spectrum in singularly continuous. This self-dual case leads to global scaling properties of the spectrum with a range of scaling indices and an associated multifractal character [8]. These authors have also shown that, if Q is a rational approximant of an irrational number, e.g. $Q = F_{l-1}/F_l$, where F_l is the l-th Fibonacci number, then the spectrum consists of F_l bands and F_{l+1} gaps.

The simple Aubry model in one dimension does not have a mobility edge, whereas an extension due to Griniasty and Fishman [9] seems to have an extended-localised transition at an appropriate mobility edge under certain circumstances. For this model, which is sometimes called the Harper model, $\varepsilon_n = \lambda \cos(2\pi n^{\gamma} Q + \delta)$ and $\gamma \neq 1$. For $\gamma \geq 2$, it has been stated that the problem is equivalent to the corresponding random problem [15] and all states are exponentially localised. It may be noted that $\gamma \neq 1$ gives rise to an inhomogeneity in the period of the potential. It is known that inhomogeneity in the amplitude variation of the potential gives rise to localisation-delocalisation transition [16]. It will be interesting to study whether such an effect arises out of inhomogeneity of the period of the potential. The idea of inhomogeneity of the period may be easily noted if we write the potential as $\lambda \cos[2\pi n\,(Qn^{\gamma-1})]$. The effective period $Q' = Qn^{\gamma-1}$ is n dependent, and so inhomogeneous.

Griniasty and Fishman [9] studied the band centre states for $0 < \gamma < 1$ with Q irrational within the perturbation theory and concluded that all states are extended. In contrast Das Sarma *et al*, [10] observed, using a heuristic argument and exact numerical calculations of eigenvalues and wave amplitudes in finite systems, that for $0 < \gamma < 1$, $\lambda < 2$ there are mobility edges at $E_c = \pm (2V - \lambda)$, with extended states at the centre of the band $|E| < (2V - \lambda)$ and localised states at the band edges $(2V - \lambda) < |E| < (2V + \lambda)$. Further for $1 < \gamma < 2$ they find along with Thouless [17] that all states away from the exact band centre are localised and the Lyapunov exponent (inverse localisation length) approaches zero extremely slowly at the band centre.

Our aim is to study wave propagation in such models by numerically calculating the transmittance as a function of the energy of the incident wave and by monitoring the way in which the phase of the transmission coefficient (which is related to the phase of the electronic wave function) changes as the wave propagates through the medium. This will be done for all values of γ including negative values not explicitly reported so far. Our approach based on the vector recursion technique of Godin and Haydock [1] is complementary to that of Das Sarma *et al* [9]. The vector recursion method, as we shall indicate, is easily extended to more than one dimensions : a work which we shall report in a subsequent communication. Our results are, to a large extent, in agreement with those of Das Sarma *et al* [10], justifying their criticism of the earlier of Griniasty and Fishman [9].

The results we report [18] except those on Argand maps of the complex transmission coefficient, are to a large extent complementary to those of Das Sarma *et al* [10]. The recursion method has the great virtue of giving a measurable quantity (namely, the transmittance) and the mobility edges can be located relatively easily with smaller size systems by looking at the transmittance rather than by first exactly diagonalizing the Hamiltonian for a much larger system and then by calculating the Lyapunov exponent (or inverse localization length) from the eigenenergies or the eigenfunctions. As an added advantage, since the transmission coefficients contain information on the wave function at a

particular energy, one can monitor the change of the electronic phase at successive scatterings. Further, since using the transfer matrix method and applying Landauer formula one can calculate the conductance directly as a function of length, one can check the validity of the one-parameter scaling theory. One may also study the form of the renormalization group flow within this one-parameter scaling and locate its fixed-point (or points, if there is more than one). This we shall discuss in a subsequent paper. For all the results presented below, the non-random hopping term has been set at $V = 1$. Most of our calculations are done on chains of length 10^5.

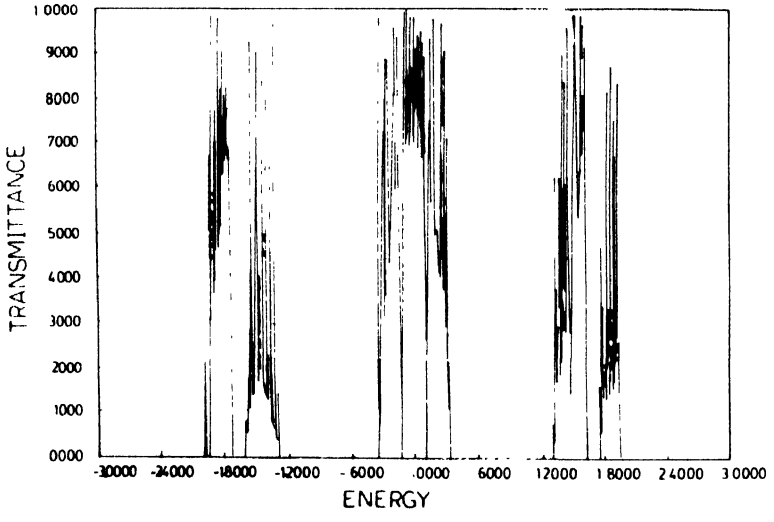

Figure 1(a). Transmittance versus energy of the incoming wave (in units of the overlap term V) for the Aubry model for $\lambda = 1$

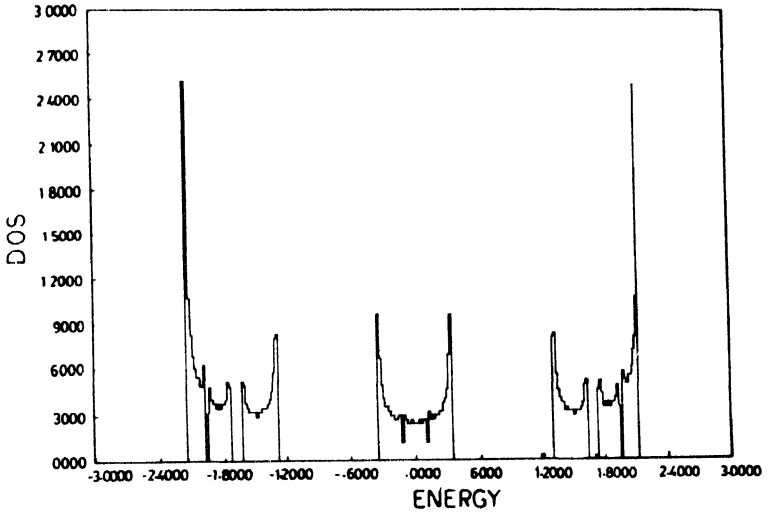

Figure 1(b). The density of states (states / atom-spin) for the Aubry model $\lambda = 1$.

Figure 1(a) shows the transmittance *versus* energy of the incoming wave for the pure Aubry model ($\gamma = 1.0$) with $\lambda = 1$. The transmittance fluctuations characteristic of incommensurate systems are clearly visible. These, in turn, lead to strong fluctuations in conductance with changes in the chemical potential [11]. In Figure 1(b), we show the density of states (DOS) for the same situation. The DOS strongly resembles that of a model where the site diagonal terms are in a Fibonacci sequence. In the Aubry model, the site-diagonal terms are incommensurate with the underlying lattice. However, the qualitative features of DOS (e.g., the gap structures) do not seem to be very different in these two cases. These two figures together show that *all* states are extended in this case. This is consistent with the fact that in the Aubry model there is an energy-independent metal-insulator transition at $\lambda = 2$, which separates the region $\lambda < 2$ where all states are extended and $\lambda > 2$, where all states are localized.

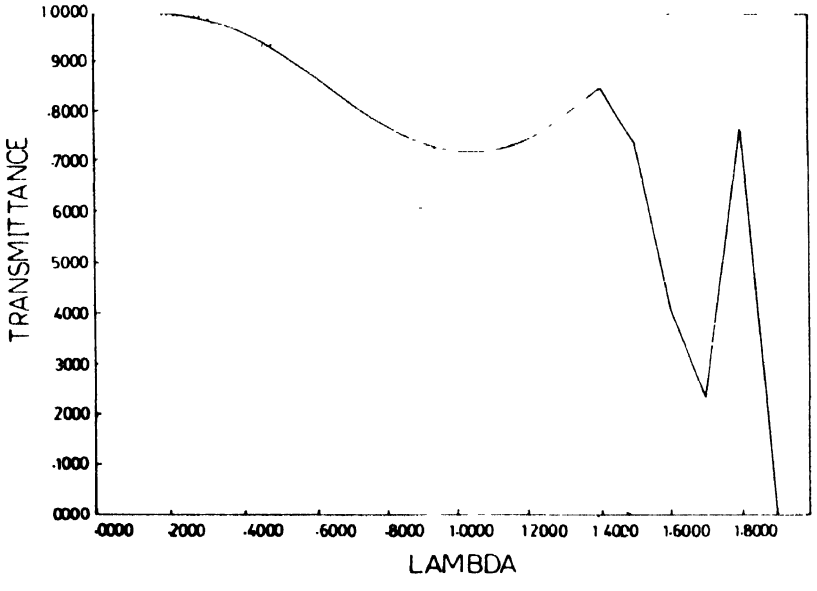

Figure 2. Transmittance at $E = 0$ (full curve) and at $E = 0.5$ (dotted curve) (E measured in units of V) for the Harper model with $\gamma = 0.5$, as a function of λ

Figure 2 shows the transmittance at the band centre $E = 0$ (full curve) and at $E = 0.5$ (dotted curve) of a more general Harper model with $\gamma = 0.5$ as a function of λ. At $\lambda = 0$ (*Bloch case*) $T(E) = 1$ as expected for both the energies. $T(E) \to 0$ as $\lambda \to 2$ for both the energies. For $E = 0.5$, $T(E)$ becomes very small beyond $\lambda = 1.5$ but truly vanishes only for $\lambda > 2$. This shows very clearly that for the Harper model with $0 < \gamma < 1$, there exist mobility edges with $E_c = \pm (2V - \lambda)$. Since in this plot we have fixed E, and plotted only positive λ's, this shows up as the existence of a metal-insulator transition at $\lambda_c = (2V - E)$. The existence of very small values of the transmittance for $\lambda > 1.5$ for the $E = 0.5$ case is simply due to finite-size effects. Below $\lambda \equiv 1.49$ the logarithm of the transmittance is virtually independent of size. Around $\lambda = 1.49$ the transmittance drops exponentially showing

exponential localisation and with an exponent increasing with size. *We should emphasize here that this method of location of the metal-insulator transition is computationally easy and fast (taking CPU time 21.75 secs on a HP 9000/300 desktop computer for a single value of λ or E and a system size of 10^5) and does not require cumbersome formulae for calculating the localisation length involving diagonalisation of very large matrices, and assumptions of exponential localisation. Indeed, as seen from Figure 2, we need not go to system sizes larger than 10^4 for locating the mobility edges. Moreover, we may use our methodology to analyse situations where we have non-exponential localisation.*

Figures 3-5 show the DOS and the transmittance as a function of energy for the Harper model with $\lambda = 1$ and $\gamma = 0.7$, 0.5 and –2.0 respectively. In the first two cases there exist mobility edges at $E_c = \pm 1$ since $V = \lambda = 1$. The case of negative γ needs special mention and we do that later on. In Figures 3 and 4 the non-analyticity of the DOS in the localised regime is evident from the rapid fluctuations in that region in contrast to the relatively smooth behaviour in the extended regime. This contrast is more apparent in the Figure 3 ($\gamma = 0.7$) than in Figure 4 ($\gamma = 0.5$) since the localisation length tends to infinity as $\gamma \rightarrow 0$ (*Bloch case*). Das Sarma *et al*'s [10] more elaborate DOS calculations on much larger systems are qualitatively similar although they show the unsmooth behaviour in the localised regime with an integrable divergence at E_c, much more transparently.

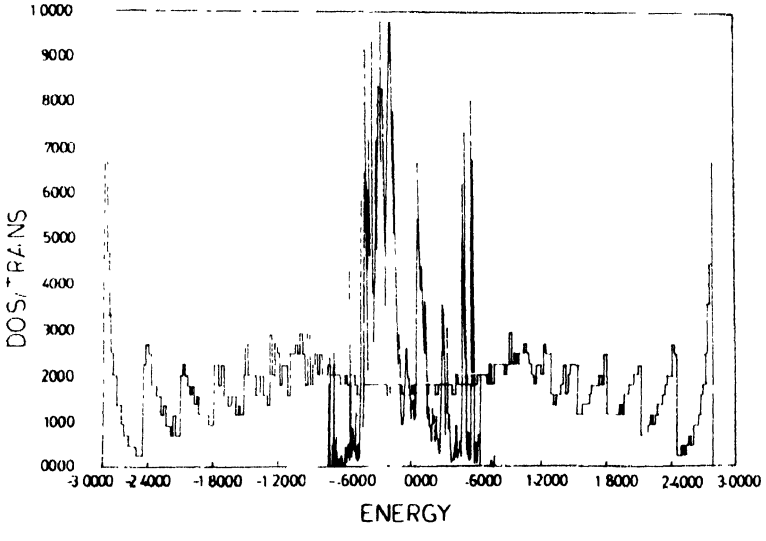

Figure 3. The density of states (states per atom-spin, scaled up by a factor of 10) and the transmittance *versus* energy, for the Harper model with $\gamma = 0.7$ and $\lambda = 1$. Mobility edges are clearly seen

Let us discuss the location of band and mobility edges for the Harper model. We can easily understand this from the following discussion put forward by Das Sarma *et al* [10] for positive γ models. Let us first note that

$$d\varepsilon_n/dn = -\{ 2\lambda\gamma\pi Q n^{\gamma-1} \sin(2\pi n^{\gamma} Q) \} \qquad (12)$$

For all $\gamma < 1$, this vanishes as $n \to \infty$, since $|\varepsilon_{n+1} - \varepsilon_n| \sim O(n^{\gamma-1})$, that is, *locally* the ε'_ns do not change much. If one assumes that the wavefunction amplitudes $\phi_n \sim z^n$, then substituting this in the Schrödinger equation, one obtains

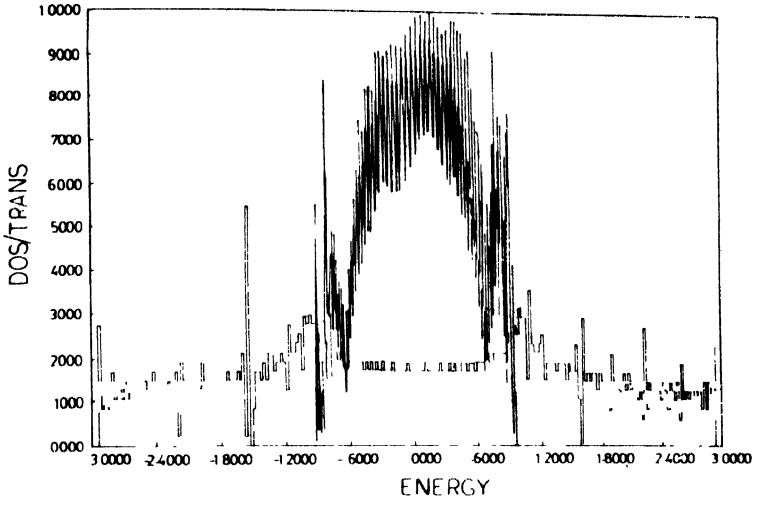

Figure 4. The same as in Figure 3 with $\gamma = 0.5$

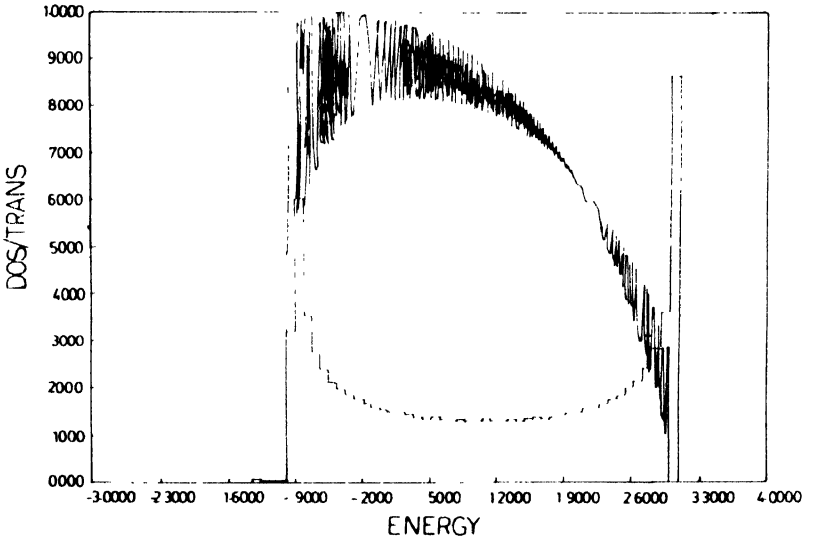

Figure 5. The same as in Figure 3 with $\gamma = 2$

$$z^2 - C_n z + 1 = 0. \tag{13}$$

where $C_n = E - \varepsilon_n$. If ${C_n}^2 \leq 4$, then z is complex, and $|z| = 1$ as appropriate for extended states. For large n, although ε_n is *locally* constant, it can take any value between $-\lambda$ and $+\lambda$ for the case $0 < \gamma < 1$. Thus if the maximum possible *positive* value of C_n, namely $(C_n)_{\max} \equiv (E + \lambda) \leq 2$, i.e. if $E \leq (2 - \lambda)$, then the condition of complexity of z is satisfied for *all*

large n. Similarly, if the minimum possible negative value, $(C)_{min} \equiv (E - \lambda) \leq -2$, i.e. if $E \geq -(2 - \lambda)$, again the condition of complexity of z is satisfied for all large n. Thus for $0 < \gamma < 1$, the mobility edges were earlier [10] predicted to be at $\pm(2 - \lambda)$, while band edges are at $\pm(2 + \lambda)$. We see from Figures 3 and 4 that, although the effect of the metal-insulator transition clearly shows up on the transmittance as a function of energy, finite size effects cause the DOS to shrink inside the band edges, particularly as $\gamma \rightarrow 1$.

We discuss the case of negative γ somewhat more elaborately since it does not seem to have been mentioned in the literature before. We see in Figure 5 for the case $\gamma = -2.0$, that the DOS has a centre shifted to $E = \lambda$ and the mobility edges are at $(-2 + \lambda)$ and $(2 + \lambda)$. This asymmetric shift of the centre is common to Harper model with all negative γ (in the large length limit).

For the case $\gamma < 0$, the argument of the trigonometric functions in eq. (13) and in the model potential approaches zero for large n. Thus, for negative values of γ and large n, the site-energies ε_n do not alternate in sign and approach a globally constant value of $+\lambda$, the approach being more rapid for larger absolute value of γ. Thus, asymptotically, the band edges shift to $-(2 - \lambda)$ and $(2 + \lambda)$, with the band centre being shifted to λ (in comparison to the case of positive γ, where the band centre was at 0). It may be noted that for small values of n close to the origin, the site energies have not yet reached the constant asymptotic value and hence given rise to some band states in the domain $[-(2 + \lambda), -(2 - \lambda)]$, but the weightage of these states in the DOS become smaller and smaller for larger and larger size chains. This is the reason why we can see a few states in the DOS of Figure 5 ($\gamma = -2.0$ and $\lambda = 1$) between $E = -3.0$ and $E = -1.0$. As for the condition for complexity of the solutions for z, we now have $(E - \lambda)^2 \leq 4$. Thus, the mobility edges are at $-(2 - \lambda)$ and $(2 + \lambda)$. Thus *asymptotically almost all* states are extended for $\gamma < 0$, even though for finite size chains this statement is not exact. It is thus interesting to note here that for $\gamma = 0$, all states are extended (*Bloch states*), but such is not the case for $\gamma > 0$. Thus $\gamma = 0$ seems to be a singular point.

One of the statements often made in that localisation results from the randomisation of the phase of the wavefunction as it travels through the system. To study this phenomenon for the present model, in Figure 6 we have plotted the Argand map of the complex transmission coefficient, i.e. its imaginary versus the real part, as the size of the system varies. This is directly related to the Argand map of the outgoing wavefunction.

At $\lambda = 1$ for $\gamma = 1$, we have a reasonably well transmitting state (Figure 6(a)). The Argand map is a regular curve with a few Fourier components. As λ increases, the maps pick up more Fourier components and resemble more complicated Lissajous' figures. The scatter about the base curve also increases. The average absolute amplitude remains reasonably close to 1, as is seen from Figure 6(a) with λ upto 1.8. Around $\lambda = 2.0$, the transmittance precipitately goes down to zero, and the Argand maps collapse to a point for $\lambda \geq 2.0$ for large enough lengths [Figure 6(b)].

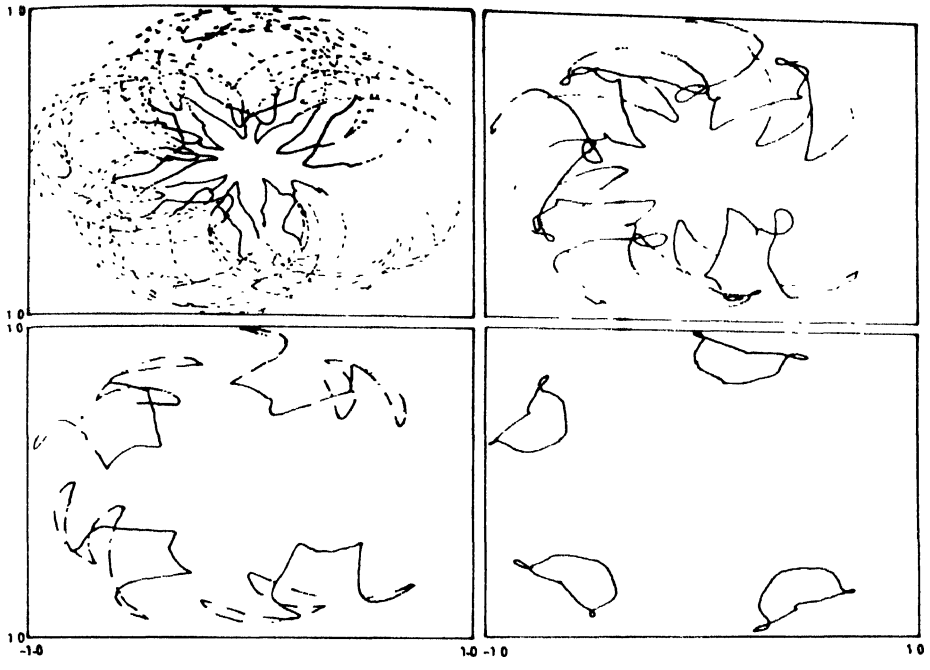

Figure 6(a). Argand maps of the complex transmission coefficients for the Aubry model at $E = 0$ (in units of V) and $\lambda = 1.0, 1.4, 1.6$, and 1.8 (clockwise)

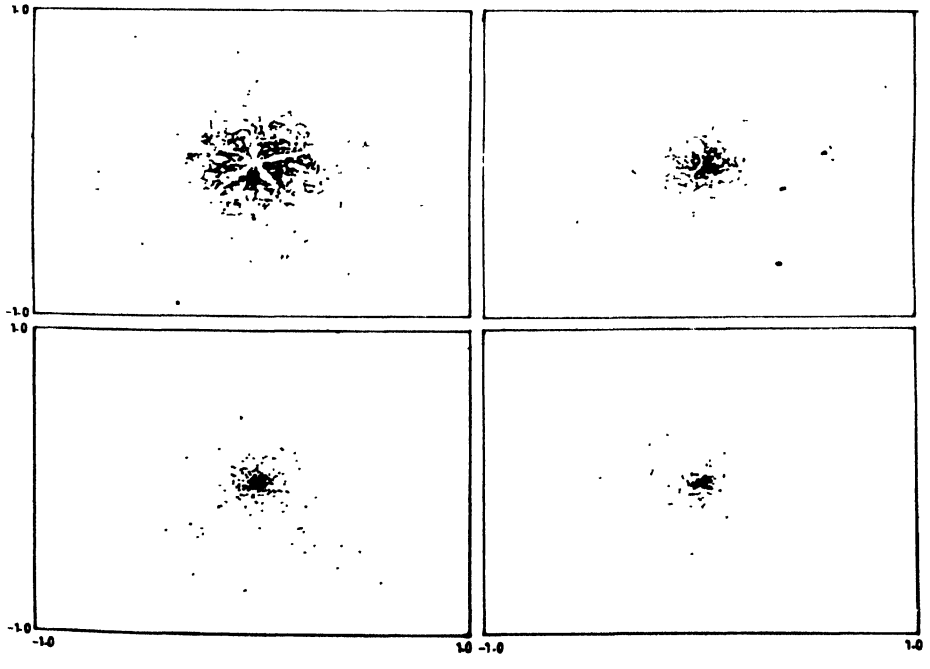

Figure 6(b). Same as in Figure 6(a) with $\lambda = 1.95, 1.98, 2.0$ and 2.02 (clockwise) where $\lambda_c = 2.0$.

3.2. Azbel resonances

It has been known for some time that in tight-binding, one-dimensional chains with short ranged overlap integrals, the electronic spectrum is a dense, point set; *almost all* of which supports exponentially localised states. The existence of a few transmitting states have also been known for some time. These are the so called **Stochastic** Resonances or Azbel Resonances [19-22]. Pendry [23] examined the reasons for the existence of these resonant states. He speculated that these states could be *necklace states*. That is, a linear combination of a number of localised states almost degenerate in energy, but whose centres of localisation are at different parts of the chain. They have sufficient overlaps between themselves and together *span* the chain. Azbel and Soven [24] had earlier estimated the width of these resonances and the way in which these scale with the sizes of the chains.

Since the width of the Azbel resonances decreases with length as exp $(-2L/\xi)$ where ξ is a measure of the localisation length, the search for Azbel resonances begin with quite small chains. For small chains, states at several energies will show large transmittance. Many of these are actually localised states whose localisation lengths are larger than the chain length. As we increase the length of the chain most of these states no longer show non zero transmittance. However, even at quite large lengths some transmitting states remain. These are the Azbel resonances. The neighbourhood of these energies are then searched for very large lengths carefully and at a very fine energy mesh to locate the position of the resonances.

For diagonal disorder $\epsilon_n = \delta(\xi_n - 0.5)$ and all the $V_n = 1$. ξ'_n s are *independent* random variables uniformly distributed between 0 and 1. δ is a measure of the strength of the disorder in the system and the energy is scaled in units of V in this case.

The transmitted wave is $\psi_N(E) = t_N \psi_o(E)$, so that $t_N(E)$ carries the information about the relative amplitude and phase of the transmitted wave for a sample of size N. The set $\{ T_N(E) = |t_N(E)|^2 \}$ then represents a set of measurements on a collection of chains of varying sizes $\{n\}$. The chain of size $n+1$ is identical to the chain of size n upto the n-th element. Note that this set is different in essence from the wavefunction amplitudes at different sites of a single isolated chain. For the multifractal analysis we shall use this set of transmittances properly normalised. Again, this analysis is different in essence from the multifractal analysis of wavefunction amplitudes for isolated chains.

The Q-th moment of this distribution for any real value of Q is

$$Z(Q) = \sum_{n=1}^{2N} P_n^Q \tag{14}$$

where $P_n = T_n(E)/T$ and $T = \Sigma T_n(E)$. This Q-th moment is also called the partition function of the distribution [25].

The indices $\tau(Q)$, α and $f(\alpha)$ are defined by the asymptotic behaviours :

$$Z(Q) \sim N^{-\tau(Q)}, P_N \sim N^{-\alpha}$$

and the fraction of atoms having exponents between α and $\alpha + d\alpha$ is $N^{f(\alpha)}$.

The three exponents $\tau(Q)$, α and $f(\alpha)$ are related to each other by

$$\tau(Q) = \alpha.Q - f(\alpha) = (Q - 1) D_Q \tag{15}$$

D_Q is referred to as the generalised (Rényi) dimension of index Q. As can be easily seen from (6) $\alpha = d\tau/dQ$. The curvature of the $f(\alpha)$ curve is $C = \left(\frac{d^2 f}{d\alpha^2}\right)_{\alpha=\alpha_0} = \frac{1}{\left(\frac{d^2\tau}{dQ^2}\right)_{Q=0}}$

Non divergence of the curvature is a signature of genuine multifractality.

For numerical facility α and $f(\alpha)$ can also be computed directly avoiding numerical differentiation [26]

$$\alpha = \frac{Z'(Q)}{Z(Q)\ln(2N)} \quad \text{and} \quad f(\alpha) = \frac{1}{\ln(2N)}\left(\ln Z(Q) - \frac{QZ'(Q)}{Z(Q)}\right) \text{ and the}$$

expression for C [27] is

$$\frac{1}{C} = \frac{1}{\ln(2N)}\left(\frac{Z'(0)^2}{Z(0)^2} - \frac{Z''(0)}{Z(0)}\right) \tag{16}$$

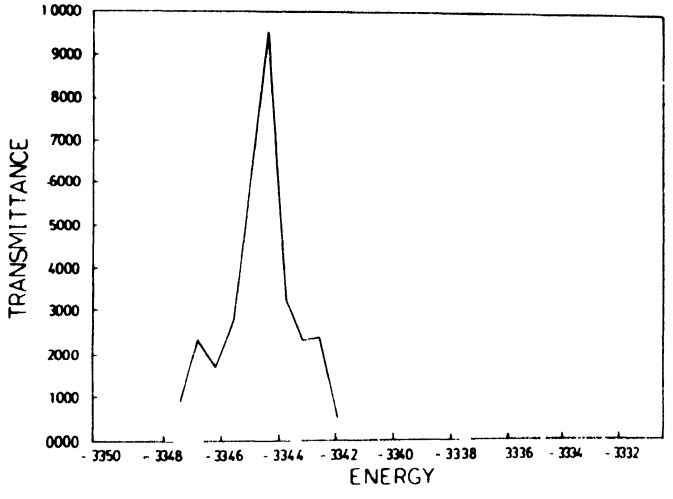

Figure 7(a). Transmittance *versus* energy (in units of V) for a chain of size 30,000 (in units of lattice spacing)

We have studied transmittance *versus* the energy of the incoming electron E, numerically to obtain the resonant states. The width of the resonance peaks get narrower as the sample length is increased. Figure 7 shows the position of the Azbel resonance for an Anderson model with purely diagonal disorder. The resonance peak sharper as the length is increased from 30,000 (in Figure 7a) to 40,000 (in Figure 7b). The states, over a very narrow energy region are transmitting while all the rest are localised. As seen in these figures, the resonant state persists with increasing length but the energy at which resonance occurs tend to shift. For the length 30,000 the resonance is at $E = -0.3344$ while for the length 40,000 it occurs at $E = -0.3385$.

Figure 8 shows the transmittance plot for Azbel resonant states. In both the length scales, the transmittance remains finite in most parts of the sample size. The sample is connected to perfectly conducting leads on both sides. So the transmittance at the incoming

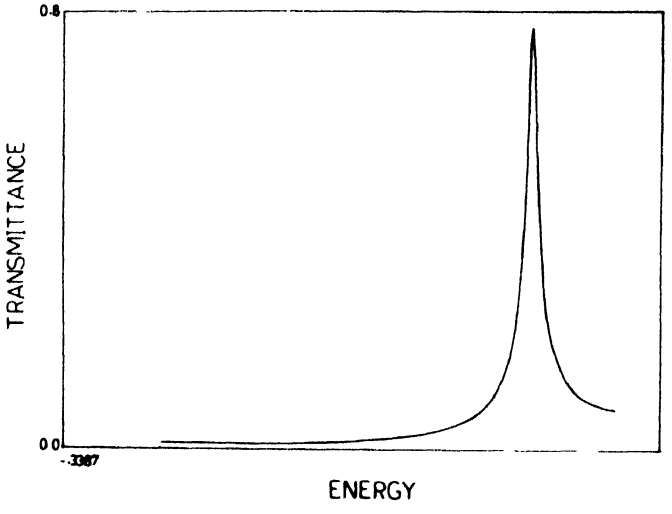

Figure 7(b). Transmittance *versus* energy (in units of V) for a chain of size 40,000 (in units of lattice spacing)

end is always equal to 1. Figure 8a shows the transmittance at an Azbel resonance in a sample of length 30,000, while Figure 8b shows the transmittance at the shifted Azbel

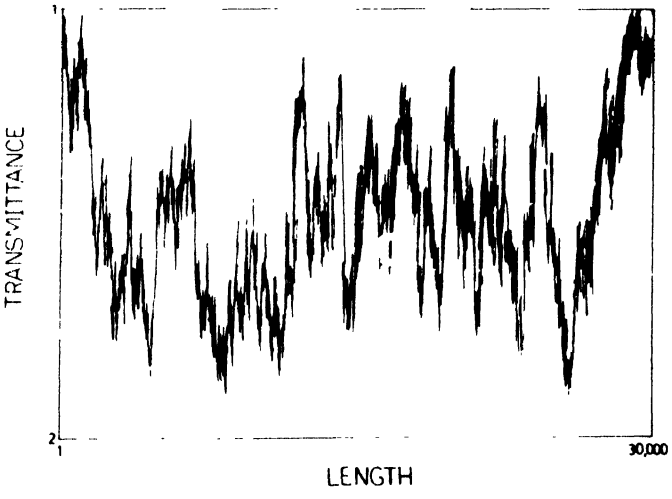

Figure 8(a). Transmittance plotted against chain length (in units of lattice spacing) for an Azbel resonant energy in a chain of length 30,000.

resonance in a sample of length 40,000. Figure 8c shows the same for a localised state in a sample of length 100,000. Here the incoming lead has transmittance equal to 1 and this falls off exponentially as the wave travels through the sample. The wave is localised within a

small length region from the incoming sides. In contrast to Figure 8a and Figure 8b except for a small mesoscopic regime the transmittance rapidly goes to zero.

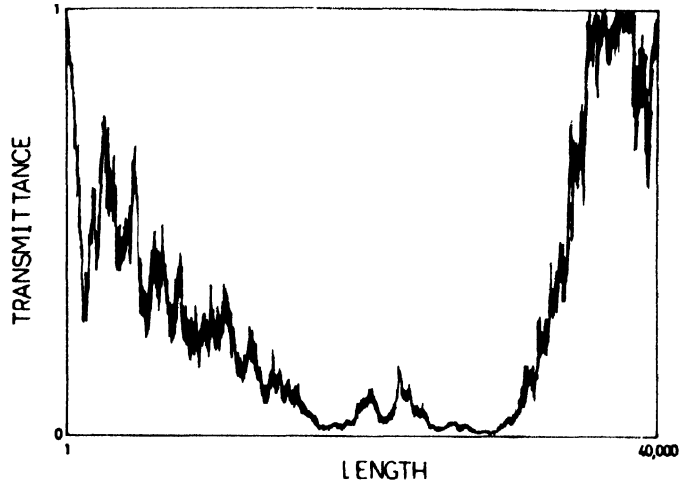

Figure 8(b). Transmittance plotted against chain length (in units of lattice spacing) for the shifted Azbel resonant energy in a chain of size 40,000.

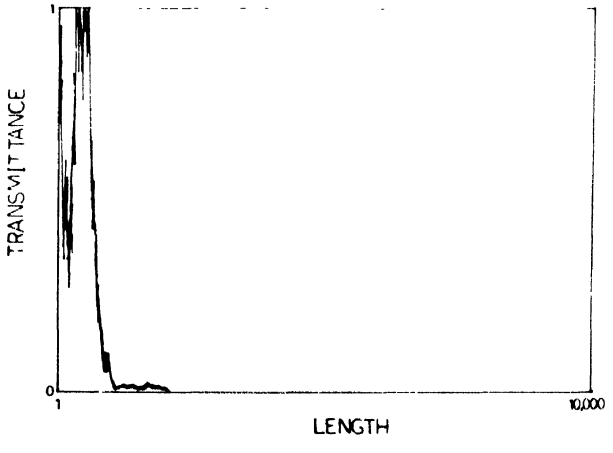

Figure 8(c). Transmittance plotted against chain length (in units of lattice spacing) for a localised state in a chain of length 100,000.

The transmittances in these disordered samples show very large fluctuations from size to size and are highly fragmented. One of the powerful methods of analysing such fragmented objects is through multifractal analysis described earlier [25].

Figure 9 shows $\tau\,(Q)$ *versus* Q graph for all three types of states : extended, localised and Azbel. For the extended state, the graph is a straight line with an almost constant slope denoted by the dashed lines here. For a localised state, the graph consists of two separate straight lines of different slopes for +ve and –ve values of Q, continuous at

$Q = 0$. This is shown by the dash-dot lines. For the Azbel state, the graph is a straight line with a constant slope. Its slope is different from the extended case. It is denoted by a solid line in the figure. For extended states $P_n \sim 1/N$, so that $Z(Q) \sim N^{1-Q}$. This leads to $\tau(Q) = Q - 1$, which is a straight line with unit slope. For localised states P_n is significantly non-zero only in an interval of size L. For positive and increasing Q the size

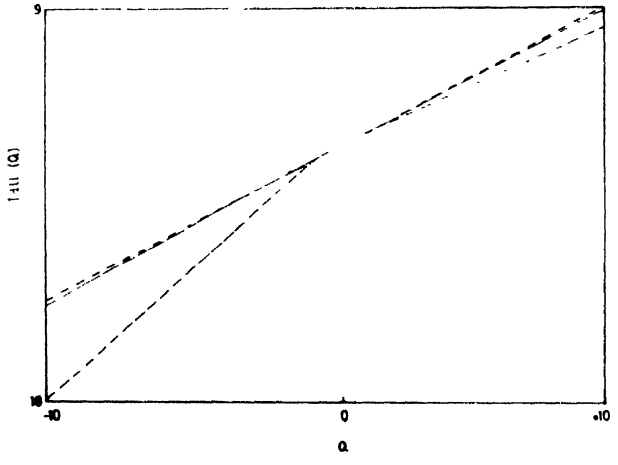

Figure 9. The scaling index $\tau(Q)$ *versus* Q for extended localised and Azbel state

of the interval over which P_n^q is significantly non-zero ($L(Q)$) decreases as Q increases. $Z(Q) \sim L^{1-q}$, $\tau(Q) \sim (1-Q)\left(\frac{\ln L(Q)}{\ln N}\right)$. The slope of this curve decreases from unity with increasing positive Q value. For negative and large $Q = -Q'$, $P_n^{Q} = P_n^{Q'}$ is now large over that interval over which P_n is almost zero. If we estimate P_n in the intervals of width ε, then $Z(Q) \sim N'(\varepsilon)^{-Q'} \sim N^{-\tau}$.

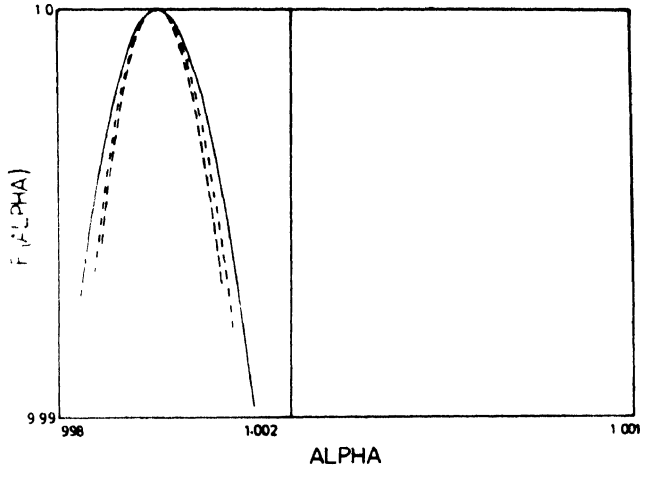

Figure 10(a). The multifractal spectrum $f(\alpha)$ *versus* α for various lengths for an extended state.

$$\tau(Q') = Q' \left(\frac{\ln \varepsilon}{\ln N}\right) - \frac{\ln N'}{\ln N}, \text{ where } N' = N - L(Q).$$

This is large and negative as ε is small. These characteristics are clear in Figure 3. Particularly in this respect the Azbel states resemble extended states. We expect this, as the nature of the localised states of being non-zero in a small interval, which is reflected in the $\tau(Q)$ *versus* Q graphs is not shared by the Azbel states. However the slope for the Azbel state curve is not unity, since the states do not possess translational symmetry and $P_i \neq (1/N)$.

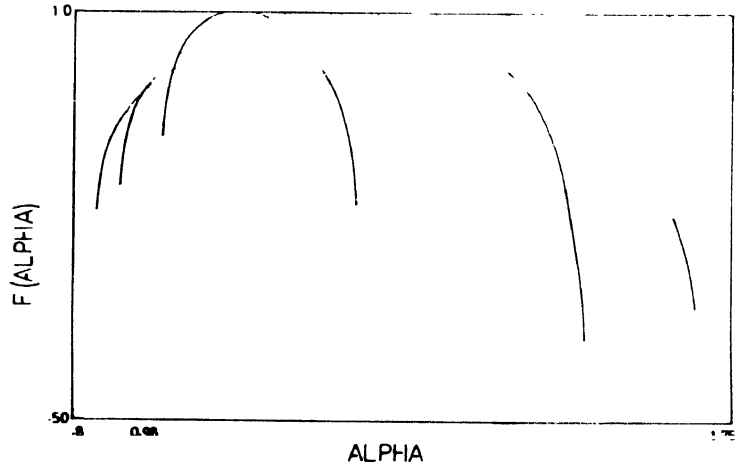

Figure 10(b). The multifractal spectrum $f(\alpha)$ *versus* α for various lengths for a localised state

Figure 10 shows $f(\alpha)$ *versus* α curves for extended, localised and Azbel states at different sample lengths. Since numerical work is always carried out on finite samples, the study of the asymptotic behaviour of the α $f(\alpha)$ curves as the size increases is very important.

Figure 10a shows the graph for an extended state. The state is for $\delta = 0.01$ and $E = 0$. For one-dimension no true extended states exist for $\delta > 0$, but for this weak disorder and energy, the state has a localisation length >> 30,000, the maximum size taken and for these lengths conveniently mimic extended states. For almost all values of Q, $f(\alpha)$ and α has values ~ 1. The interesting point here is the behaviour of the graphs as we increase the length of the sample. For a sample of length 10,000 the $f(\alpha)$ *versus* α curve is the outermost solid line curve. The curve converges inwards as the length of the sample increases to 20,000 and 30,000 respectively. For larger lengths the curve will converge to the point (1, 1).

Figure 10b shows the graph for a localised state. Here the curves move outwards as we increase the length scale. The interesting point to observe is that the density of points near α_{min} and α_{max} is very high whereas the intermediate region is sparsely populated. This

indicates clearly the fact that for exponential localisation, α_{min} becoming smaller and smaller corresponds to a large probability (which should ideally be ~ 1) for getting the electron within the localisation length. α_{max} becomes larger and larger implying that probability decays exponentially for lengths larger than the localisation length. The asymptotic convergence is at the point (0, 0) and (∞, 1).

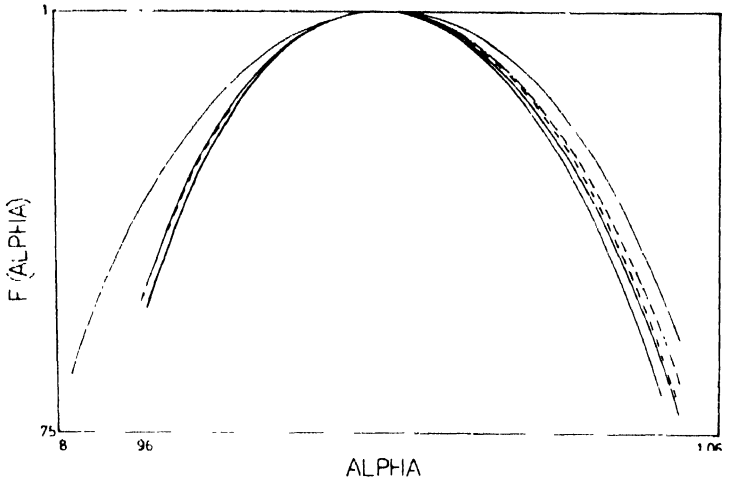

Figure 10(c). The multifractal spectrum $f(\alpha)$ *versus* α for various lengths for an Azbel state

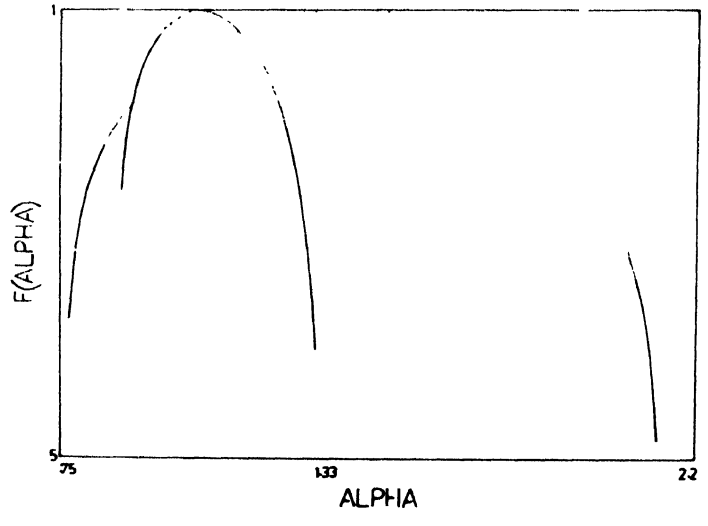

Figure 10(d). The multifractal spectrum of $f(\alpha)$ *versus* α for a localised state and an Azbel state.

Figure 10c shows the same for an Azbel state. Here the graphs are spread out, with a significant ($\alpha_{max} - \alpha_{min}$) as compared to the extended state though the peak still occurs at (≥ 1, 1). The behaviour of the graph with increasing lengths is however significantly different from the extended or localised case. Here the α_{max} and α_{min} oscillate about some

mean position. The graph moves significantly inside as the length is increased from 5000 to 10,000. But after that increase in length scale results in close overlap on the α_{min} side but having a small oscillation on the α_{max} side. As seen with increasing N the Azbel state show finite (α_{min}, α_{max}). Unlike the extended state $\alpha_{min} \neq \alpha_{max}$ and unlike localised states α_{max} is finite. The true multifractal nature of the Azbel states resemble more closely the critical states in incommensurate systems.

Figure 10d compares the $\alpha - f(\alpha)$ curves of a localised state and an Azbel state. As seen, the density of points in the curve for the Azbel state is uniform whereas for the localised state the points are concentrated at the two ends.

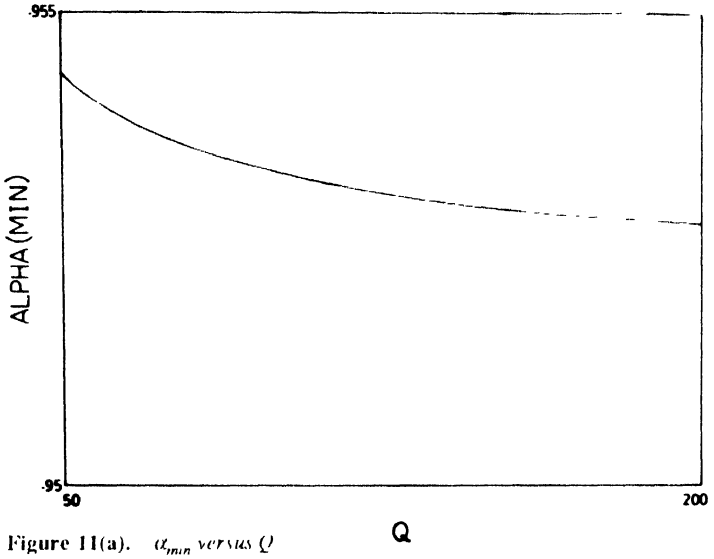

Figure 11(a). α_{min} *versus* Q

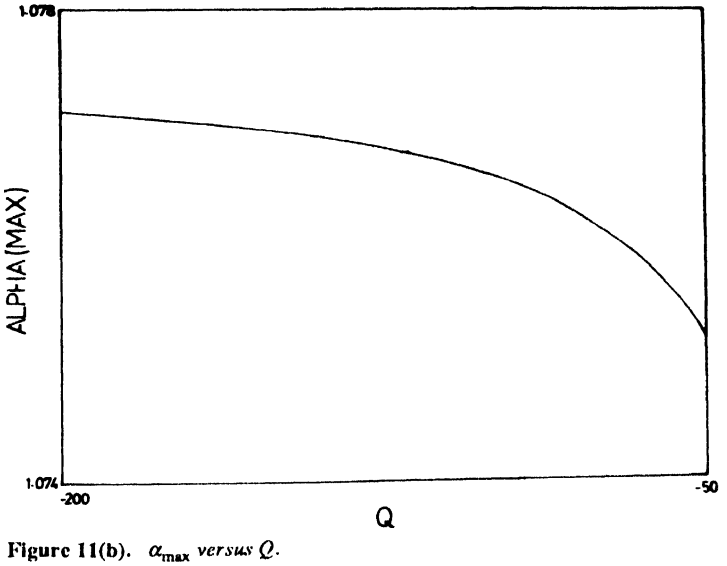

Figure 11(b). α_{max} *versus* Q.

Figure 11 shows the behaviour of α_{min} and α_{max} for an Azbel resonant state with increasing Q. Q is varied from 50 to 200 in Figure 11a. α_{min} decreases in the begining but approaches a constant value for $Q \geq 110$. Figure 11b shows Q variation from –50 to –200 to estimate α_{max}. As expected α_{max} increases with increase in –ve Q value and reaches a fixed value from about $Q = -120$.

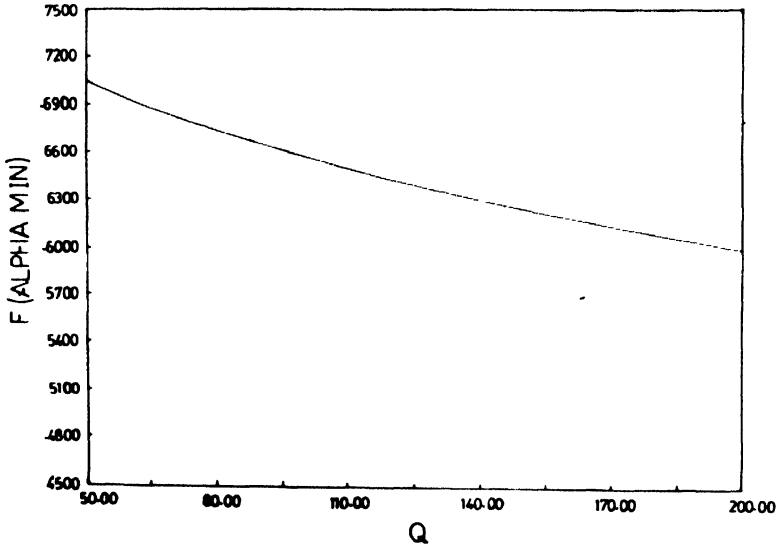

Figure 12(a). $f(\alpha_{min})$ *versus* Q.

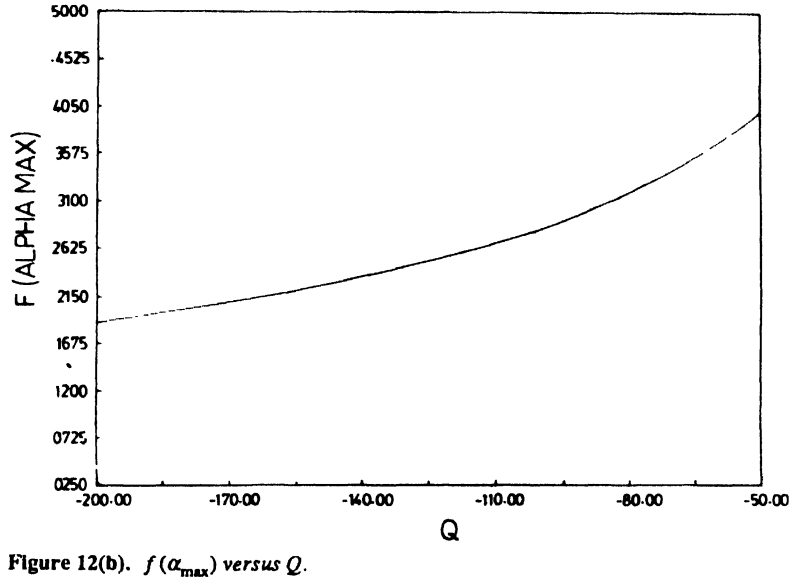

Figure 12(b). $f(\alpha_{max})$ *versus* Q.

Figure 12 shows the behaviour of $f(\alpha_{min})$ and $f(\alpha_{max})$ with increasing Q for Azbel resonant state. Figure 12a has Q variation from 50 to 200 to find $f(\alpha_{min})$. Figure 12 has Q

variation from –50 to –200 to find $f(\alpha_{max})$. f decreases for both large +ve and –ve values of Q. $f(\alpha_{max})$ decreases more sharply than $f(\alpha_{min})$, going towards zero for large –ve Q values. However any further increase in Q value brings in numerical instability and to overcome this, quadruple precision, not available with us, has to be used .

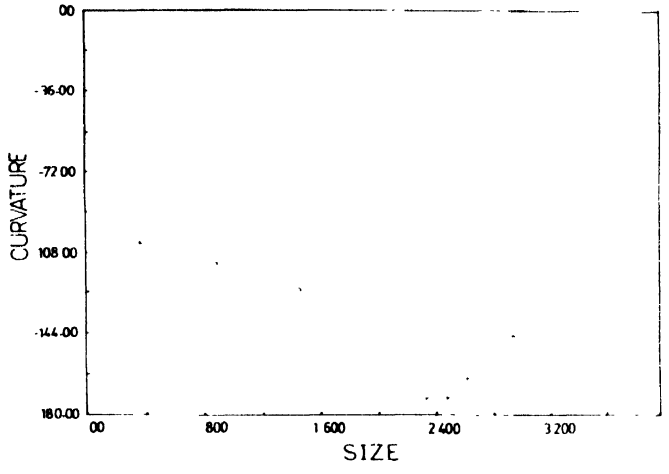

Figure 13(a). The curvature C *versus* the chain size

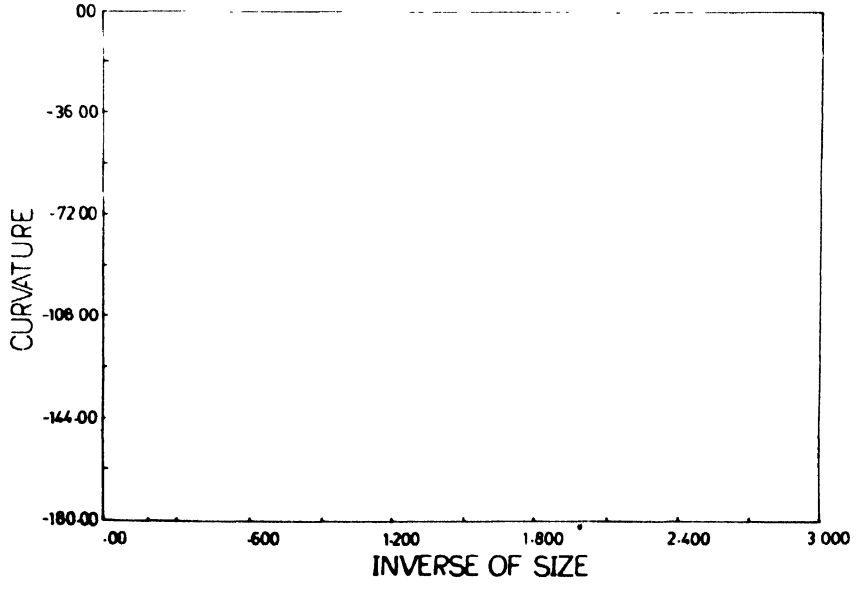

Figure 13(b). The curvature C *versus* the inverse of the chain size

Figure 13 shows the curvature for the multifractal analysis of the transmittances at Azbel resonance. Figure 13a gives curvature C *versus* $2N$, the sample size. Figure 13b gives